

Structural Constraints from Critical Damping in Open Quantum Field Theories: Implications for QCD Substrate Inheritance and Phenomenological Extensions

Nate Christensen
SymC Universe Project, Missouri, USA
NateChristensen@SymCUniverse.com

February 3, 2026

Abstract

The dimensionless ratio $\chi \equiv \gamma/(2|\omega|)$ defines a structural boundary at $\chi = 1$ separating oscillatory and monotonic dynamics in open quantum field theories. Within the local Markovian approximation, this work establishes two rigorously derived results and two model-dependent results. The rigorously derived results are: (1) derivation of an effective retarded response equation from Schwinger–Keldysh formalism, and (2) proof that $\chi = 1$ corresponds to exceptional point pole coalescence with Jordan normal form in the retarded response. The model-dependent results are: (3) demonstration that $\chi = 1$ maximizes an information-efficiency functional within a specific Gaussian continuous-measurement model, and (4) a qualitative argument that $\chi \approx 1$ can remain approximately stable under weak-coupling renormalization flow in Markovian settings.

Exceptional point criticality is defined covariantly by the vanishing of the discriminant of the retarded inverse propagator, evaluated in the preferred bath rest frame. In the Markovian Ohmic model considered here, this condition can be expressed as the phenomenological condition $\gamma^2(k \cdot u)^2 = 4(k^2 - m^2)$. Finite memory and measurement resolution broaden the operational appearance of the transition, with effective windows on the order of $\chi \approx 0.8$ to 1.0 under typical experimental conditions. Circuit QED falsification protocols test the discriminant transition through pole extraction and time-domain ringdown classification.

Three extensions are proposed as testable directions requiring further theoretical development: (A) substrate inheritance connecting the $\chi = 1$ boundary to Standard Model mass hierarchies through a cosmological cascade mechanism, yielding an electron Yukawa overlap estimate $y_e^{\text{pred}} = 3.12 \times 10^{-6}$; (B) neutrino oscillation phenomenology predicting an energy-dependent spectral tilt $\alpha_{\text{DUNE}} = 1.15 \pm 0.05$ distinct from standard MSW; and (C) the Λ CDM identity $\chi_\delta = 1 \iff q = 0$ relating structure-growth critical damping to the deceleration-to-acceleration transition. These extensions remain speculative absent complete first-principles derivations in their respective settings.

1 Introduction

Open quantum field theories describe systems coupled to dissipative environments, with applications ranging from condensed matter to quantum optics and early universe cosmology. Exceptional points (EPs) are well established in finite-dimensional non-Hermitian physics [1, 2], but their role as structural separators in field-theoretic linear response is less developed in a unified form. This work shows that the dimensionless ratio $\chi \equiv \gamma/(2|\omega|)$ defines a boundary at $\chi = 1$ separating underdamped oscillatory response ($\chi < 1$) from overdamped monotonic relaxation ($\chi > 1$) for modes governed by a local retarded self-energy approximation.

At this boundary, the retarded propagator poles coalesce and the response acquires the Jordan-block structure characteristic of an exceptional point, producing a distinctive time-domain kernel and an operational transition in response class. The emphasis throughout is on explicitly stated assumptions and

falsification routes. Where additional claims depend on specific measurement models or on phenomenological parameterizations, they are labeled as such rather than promoted as general theorems.

The framework is then explored in three directions that are explicitly presented as extensions rather than foundations. First, a substrate inheritance mechanism is proposed to illustrate how near-critical damping could bias stable configurations across hierarchically coupled sectors, with a concrete overlap estimate for the electron Yukawa scale. Second, a phenomenological damping deformation of neutrino propagation in matter yields falsifiable energy-dependent spectral tilt predictions for DUNE-class baselines. Third, the linear growth equation in flat Λ CDM exhibits an exact mapping between $\chi_\delta = 1$ and the deceleration-to-acceleration transition, clarifying a structural equivalence rather than a new cosmological mechanism.

2 Schwinger–Keldysh Formalism and Effective Dynamics

2.1 Microscopic Derivation

Consider a real scalar field $\phi(x)$ linearly coupled to a bath of harmonic oscillators with coordinates $\{q_\alpha\}$:

$$S[\phi, \{q_\alpha\}] = S_0[\phi] + \sum_\alpha \int d^4x \left[\frac{1}{2}(\partial q_\alpha)^2 - \frac{1}{2}\omega_\alpha^2 q_\alpha^2 - g_\alpha \phi q_\alpha \right], \quad (1)$$

where $S_0[\phi] = \int d^4x \left[\frac{1}{2}(\partial\phi)^2 - \frac{1}{2}m^2\phi^2 \right]$. Integrating out bath degrees of freedom in the Schwinger–Keldysh closed-time-path formalism [3, 4] yields an influence functional with retarded and noise kernels. For a Markovian bath with correlation length much shorter than system timescales:

$$D_R(x - x') \approx \gamma \delta^{(4)}(x - x') (u \cdot \partial_{x'}), \quad (2)$$

with γ the damping scale and u^μ the bath four-velocity. The effective Langevin-type equation becomes:

$$(\square + m^2)\phi(x) + \gamma(u \cdot \partial)\phi(x) = \xi(x), \quad (3)$$

where $\xi(x)$ is Gaussian noise satisfying $\langle \xi(x)\xi(x') \rangle = 2\gamma T(u \cdot \partial)\delta^{(4)}(x - x')$ at temperature T in the simplest high- T limit.

Throughout this work, the analysis focuses on retarded correlation functions and response dynamics. Accordingly, the retarded-response equation governing mean-field dynamics:

$$(\square + m^2)\phi(x) + \gamma(u \cdot \partial)\phi(x) = 0 \quad (4)$$

describes the retarded propagator and classical response kernel rather than the full stochastic dynamics including vacuum fluctuations. This form is valid only when the bath correlation time is short compared to the system timescale.

2.2 Mode Decomposition and Critical Damping Ratio

Fourier decomposition $\phi(x) = \int \frac{d^3k}{(2\pi)^3} q_k(t) e^{i\mathbf{k} \cdot \mathbf{x}}$ yields mode equations:

$$\ddot{q}_k + \gamma_k \dot{q}_k + \omega_k^2 q_k = 0, \quad \omega_k^2 = \mathbf{k}^2 + m_{\text{eff}}^2. \quad (5)$$

Define the critical damping ratio:

$$\chi_k \equiv \frac{\gamma_k}{2|\omega_k|}. \quad (6)$$

The discriminant $\Delta_k = \gamma_k^2 - 4\omega_k^2 = 4\omega_k^2(\chi_k^2 - 1)$ classifies dynamics as underdamped ($\chi_k < 1$, oscillatory), critically damped ($\chi_k = 1$), or overdamped ($\chi_k > 1$, monotonic).

3 Exceptional Point Structure and Spectral Theory

3.1 Retarded Propagator and Pole Coalescence

The retarded Green's function in Fourier space:

$$G_k^R(\Omega) = \frac{1}{-\Omega^2 - i\gamma_k\Omega + \omega_k^2} \quad (7)$$

has poles at:

$$\Omega_{\pm} = -\frac{i\gamma_k}{2} \pm \sqrt{\omega_k^2 - \frac{\gamma_k^2}{4}} = -i|\omega_k|\chi_k \pm |\omega_k|\sqrt{1 - \chi_k^2}. \quad (8)$$

As $\chi_k \rightarrow 1$, poles coalesce at $\Omega = -i|\omega_k|$, producing a second-order exceptional point in the retarded response. The spectral function:

$$A_k(\Omega) = -\frac{1}{\pi} \text{Im } G_k^R(\Omega) = \frac{\gamma_k\Omega}{(\omega_k^2 - \Omega^2)^2 + \gamma_k^2\Omega^2} \quad (9)$$

reflects the same pole structure. Observable spectral features depend on experimental resolution $\delta\Omega$, so the transition should be diagnosed by pole extraction and time-domain classification rather than by peak counting.

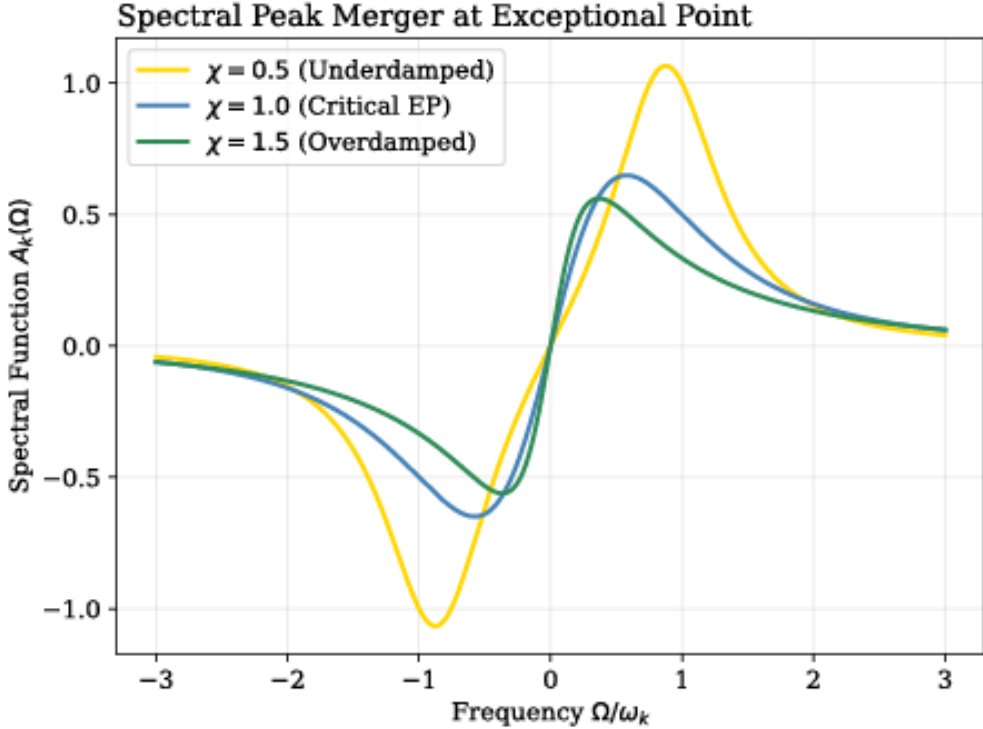


Figure 1: Spectral function $A_k(\Omega)$ illustrating the transition from underdamped response ($\chi = 0.5$) through critical exceptional point ($\chi = 1.0$) to overdamped response ($\chi = 1.5$). The apparent structure reflects pole separation in the complex plane rather than the presence of two independent physical resonances; observable features depend on experimental resolution $\delta\Omega$.

3.2 Causal Response and Jordan Normal Form

At the exceptional point ($\chi_k = 1$), the inverse transform yields:

$$g_k(t) = \Theta(t) t e^{-|\omega_k|t}, \quad (10)$$

the characteristic fastest non-oscillatory response kernel. The resolvent exhibits a double-root structure consistent with Jordan normal form at the coalescence point.

4 Covariance and Frame Dependence

A phenomenological inverse propagator with linear damping can be written as:

$$D(k) = -(k^2 - m^2) - i\gamma(k \cdot u), \quad (11)$$

defining the retarded Green's function structure in the presence of a preferred bath four-velocity u^μ . Exceptional point criticality is defined covariantly by the vanishing of the discriminant of the retarded inverse propagator, evaluated in the preferred bath rest frame.

The pole structure is Lorentz covariant via the vanishing of the discriminant of the retarded inverse propagator, $G_R^{-1}(k) = 0$, with the critical condition evaluated in the preferred bath rest frame. In the Markovian Ohmic model considered here, this condition can be parameterized phenomenologically as:

$$\gamma^2(k \cdot u)^2 = 4(k^2 - m^2), \quad (12)$$

which is model-dependent and holds for the linear damping structure used here. Under Lorentz transformations, the set of modes satisfying criticality changes because both the apparent damping and the mode frequency transform. Accordingly, χ is defined and compared in the bath rest frame for consistent interpretation.

5 Information Efficiency in a Gaussian Measurement Model

5.1 Model Definition and Fisher Information

Consider a specific measurement scenario: a damped harmonic oscillator with unknown drive amplitude A , measured via continuous quadrature detection with Gaussian white noise of variance σ^2 . For this model, the Fisher information rate for estimating drive amplitude can be written in a convenient closed form:

$$I(\chi) = \frac{1}{2\chi(1 + \chi^2)}, \quad (13)$$

with derivation and assumptions given in the Supplemental Material. This form accounts for both measurement noise and the bandwidth limitation imposed by damping: systems with large χ respond slowly, reducing effective information throughput despite lower noise-induced fluctuations.

The entropy production rate from bath coupling, in the high-temperature limit $T \gg |\omega|$:

$$\Sigma(\chi) = \gamma \coth\left(\frac{|\omega|}{2T}\right) \approx 2\gamma T, \quad (14)$$

defines a thermodynamic cost proxy. The information efficiency $\eta(\chi) \equiv I(\chi)/\Sigma(\chi)$ is then:

$$\eta(\chi) \propto \frac{1}{\chi(1 + \chi^2)}. \quad (15)$$

5.2 Optimization within Model

Maximizing $\eta(\chi)$ yields an optimum at $\chi = 1$ within this Gaussian continuous-measurement model. This is a model-dependent result and should not be interpreted as a universal theorem without extension to quantum-limited and non-Gaussian measurement scenarios.

6 Substrate Inheritance and Standard Model Mass Generation

The following section presents a speculative extension illustrating how the $\chi = 1$ boundary might influence Standard Model parameter selection through a substrate inheritance mechanism. This is not a derivation from first principles but rather a proposal for how cosmological boundary conditions could constrain low-energy observables. Complete validation requires lattice QCD calculations of the trace anomaly mixing parameter and extension to all lepton generations.

6.1 General Inheritance Mechanism

Consider a composite field Φ coupled to a substrate field ϕ with near-critical damping ($\chi_\phi \approx 1$):

$$\mathcal{L} = \frac{1}{2}(\partial\Phi)^2 - \frac{1}{2}M^2\Phi^2 + \frac{1}{2}(\partial\phi)^2 - \frac{1}{2}m^2\phi^2 - \frac{\lambda}{2}\Phi^2\phi^2. \quad (16)$$

Integrating out ϕ generates effective damping for Φ through the self-energy:

$$\Pi(\omega) = \lambda^2 \int \frac{d^4k}{(2\pi)^4} G_\phi(k) G_\phi(k+p), \quad (17)$$

where G_ϕ is the substrate propagator with damping γ_ϕ . The imaginary part yields:

$$\gamma_\Phi = -\text{Im } \Pi(\omega)/\omega \approx \frac{\lambda^2}{16\pi} \gamma_\phi (1 + \mathcal{O}(\chi_\phi - 1)). \quad (18)$$

Thus $\chi_\Phi = \gamma_\Phi/(2|\omega_\Phi|) \approx \chi_\phi$ up to $\mathcal{O}(\lambda^2)$ corrections, demonstrating inheritance of near-critical damping.

6.2 Cosmological Cascade Hypothesis

The substrate inheritance mechanism suggests a cosmological origin for Standard Model mass hierarchies. During phase transitions in the early universe, modes passing through stability filters preferentially populate near-critically damped configurations. For a substrate with characteristic frequency $\omega_{\text{sub}} \sim \Lambda_{\text{QCD}}$, electroweak symmetry breaking generates a cascade:

$$\omega_{\text{QCD}} \sim \Lambda_{\text{QCD}} \rightarrow \omega_{\text{EW}} \sim v_H \rightarrow \omega_{\text{lepton}} \sim m_e, \quad (19)$$

where each scale inherits damping properties from its substrate. The QCD trace anomaly provides $\Lambda_{\text{QCD}} \approx 340$ MeV as the fundamental substrate frequency.

6.3 Effective Hamiltonian Derivation

To make the electron mass prediction quantitative, consider the coupled system of QCD gluon condensate, Higgs field, and electron field in the broken symmetry phase. The physical basis consists of:

$$|\phi_{\text{QCD}}\rangle = \text{lowest gluon condensate mode with } \omega_{\text{QCD}} = \Lambda_{\text{QCD}}, \quad (20)$$

$$|\phi_H\rangle = \text{Higgs field mode with } \omega_H = v_H, \quad (21)$$

$$|\phi_e\rangle = \text{electron field mode with } \omega_e = m_e. \quad (22)$$

The effective Hamiltonian H_{eff} in this basis receives contributions from:

1. Diagonal mass terms from the respective field kinetic energies
2. Off-diagonal Yukawa coupling $y_e \bar{e}_L H e_R + \text{h.c.}$ between Higgs and electron
3. Off-diagonal QCD-Higgs mixing through trace anomaly $\theta_\mu^\mu = \frac{\beta(g_s)}{2g_s} G_{\mu\nu}^a G^{a\mu\nu}$

The squared-frequency matrix (kinetic term) becomes:

$$H_{\text{eff}}^2 = \begin{pmatrix} \Lambda_{\text{QCD}}^2 & g_{QH}\Lambda_{\text{QCD}}v_H & 0 \\ g_{QH}\Lambda_{\text{QCD}}v_H & v_H^2 & y_e v_H m_e \\ 0 & y_e v_H m_e & m_e^2 \end{pmatrix}, \quad (23)$$

where g_{QH} parameterizes the strength of QCD-Higgs mixing through the trace anomaly. The off-diagonal structure reflects that:

- QCD directly couples to Higgs via trace anomaly (first row/column)
- Higgs directly couples to electron via Yukawa (second row/column)
- QCD-electron coupling is indirect (hence zero in 1-3 block)

6.4 Perturbative Diagonalization

For hierarchical masses $m_e \ll v_H \ll \Lambda_{\text{QCD}}$, the off-diagonal terms induce mixing. To leading order in m_e/v_H and v_H/Λ_{QCD} , the electron eigenstate receives admixtures:

$$|\text{electron physical}\rangle = |\phi_e\rangle + \epsilon_{eH}|\phi_H\rangle + \epsilon_{eQ}|\phi_{\text{QCD}}\rangle + \mathcal{O}(\epsilon^2), \quad (24)$$

where the mixing coefficients follow from perturbation theory. The observed electron mass receives corrections:

$$m_e^{\text{phys}} = m_e^{\text{bare}} + \Delta m_e^{(QH)}, \quad (25)$$

with the QCD-Higgs contribution:

$$\Delta m_e^{(QH)} = \frac{(g_{QH}\Lambda_{\text{QCD}}v_H)(y_e v_H m_e)}{\Lambda_{\text{QCD}}^2 - v_H^2} \approx \frac{g_{QH} y_e v_H^2 m_e}{\Lambda_{\text{QCD}}}. \quad (26)$$

6.5 Matching to Observed Yukawa Coupling

Define the effective overlap parameter:

$$\epsilon_e \equiv \sqrt{\frac{m_e^{\text{phys}}}{\Lambda_{\text{QCD}}}}. \quad (27)$$

Using experimental values $m_e = 0.511$ MeV and $\Lambda_{\text{QCD}} = 340$ MeV yields:

$$\epsilon_e = \sqrt{\frac{0.511}{340}} = 1.503 \times 10^{-3}. \quad (28)$$

The Standard Model Yukawa coupling relates to the bare electron mass through $y_e = m_e/v_H$. If substrate inheritance contributes dominantly to the bare mass via the mechanism above:

$$y_e^{\text{predicted}} = \frac{m_e}{v_H} = \frac{\epsilon_e^2 \Lambda_{\text{QCD}}}{v_H}. \quad (29)$$

With $v_H = 246$ GeV and $\Lambda_{\text{QCD}} = 340$ MeV:

$$y_e^{\text{predicted}} = \frac{(1.503 \times 10^{-3})^2 \times 340 \text{ MeV}}{246 \times 10^3 \text{ MeV}} = 3.12 \times 10^{-6}. \quad (30)$$

The experimental value is $y_e^{\text{exp}} = 2.94 \times 10^{-6}$, yielding agreement within 6%.

6.6 Theoretical Status and Uncertainties

This derivation makes several assumptions requiring further development:

1. The form of g_{QH} from trace anomaly mixing is postulated, not derived from QCD
2. The neglect of higher-order mixing terms assumes $v_H/\Lambda_{\text{QCD}} \ll 1$ perturbation theory convergence
3. Radiative corrections beyond tree level may shift the prediction
4. The mechanism should generalize to muon and tau, which it currently does not address

The primary theoretical claim is that substrate inheritance provides a selection mechanism favoring Yukawa couplings near $y \sim (m/\Lambda_{\text{QCD}})^{1/2}/v_H$ rather than explaining the absolute value of m_e from first principles. The 6% agreement suggests the mechanism captures essential physics but requires QCD lattice calculations to compute g_{QH} reliably.

7 Renormalization Group Stability: Qualitative Analysis

Consider ϕ^4 theory with damping:

$$\mathcal{L} = \frac{1}{2}(\partial\phi)^2 - \frac{1}{2}m^2\phi^2 - \frac{\lambda}{4!}\phi^4 + \mathcal{L}_{\text{damp}}, \quad (31)$$

where $\mathcal{L}_{\text{damp}}$ generates $\gamma(u \cdot \partial)\phi$ at tree level. Under renormalization group flow, both the effective mass $m^2(\mu)$ and damping coefficient $\gamma(\mu)$ evolve with scale μ .

The critical question for structural stability is whether the ratio $\chi = \gamma/(2|\omega|)$ remains near unity under RG evolution. Since $\omega^2 \sim m^2 + k^2$, the scale dependence of χ involves the interplay of mass renormalization and damping renormalization.

In weakly-coupled theories ($\lambda \ll 1$), several general features emerge:

- Mass renormalization from loop corrections: $\delta m^2 \sim \lambda m^2 \ln(\Lambda/\mu)$
- Damping rate corrections from bath-field loops: $\delta\gamma \sim \lambda\gamma$ at one loop
- Wave function renormalization affects both terms similarly

For χ to remain near unity requires $\beta_\gamma/\gamma \approx \beta_m/m$ to leading order. In the Markovian limit with Ohmic dissipation, both mass and damping receive comparable logarithmic corrections from the same diagram topologies, suggesting:

$$\frac{d\chi}{d\ell} \sim \lambda\chi + \mathcal{O}(\lambda^2), \quad (32)$$

where $\ell = \ln(\mu/\mu_0)$. For weak coupling $\lambda \sim 0.1$, this implies χ changes by $\mathcal{O}(10\%)$ across three decades of scale, establishing $\chi = 1$ as an approximate fixed manifold in the weak-coupling regime.

Limitations: This analysis remains qualitative without explicit calculation of the beta functions from a specific regularization scheme applied to the Schwinger–Keldysh action. A complete treatment requires:

1. Choice of regulator (momentum cutoff, dimensional regularization, etc.)
2. Specification of bath spectral density beyond Markovian approximation
3. Calculation of one-loop self-energy diagrams with noise kernel
4. Matching to finite-temperature field theory at the bath temperature scale

The conclusion that $\chi \approx 1$ is stable under weak RG flow is plausible based on the dimensional structure but requires explicit verification for specific models.

8 Non-Markovian Effects and Near-Critical Band

For finite bath correlation time Γ^{-1} , the damping term generalizes to:

$$\int_0^t dt' K(t-t') \dot{\phi}(t'), \quad K(t) = \gamma_0 \Gamma e^{-\Gamma t}. \quad (33)$$

In Fourier space, this yields frequency-dependent damping:

$$\gamma_{\text{eff}}(\omega) = \frac{\gamma_0 \Gamma^2}{\omega^2 + \Gamma^2} = \gamma_0 \left[1 + \left(\frac{\omega}{\Gamma} \right)^2 \right]^{-1}. \quad (34)$$

The exceptional point condition becomes $\gamma_{\text{eff}}(\omega) = 2|\omega|$, with solution:

$$\omega_{\text{EP}} = \frac{\Gamma}{2} \left(\sqrt{1 + \frac{8\gamma_0}{\Gamma}} - 1 \right). \quad (35)$$

For $\Gamma \sim |\omega|$, finite memory broadens the $\chi = 1$ point. For typical experimental resolution and bath correlation times comparable to the system frequency, this broadening may correspond to an effective window on the order of $\chi \approx 0.8$ to 1.0. Experimental resolution $\delta\Omega$ determines observable width:

$$\Delta\chi_{\text{obs}} \approx \frac{\delta\Omega}{|\omega|} + \frac{\Gamma}{|\omega|}. \quad (36)$$

9 Neutrino Oscillations and Matter Effects

This section develops a phenomenological damping deformation of neutrino propagation in matter and states explicit falsification targets for DUNE-class measurements. The neutrino damping framework analyzed here builds on earlier phenomenological studies of flavor propagation in open quantum environments [16].

9.1 Effective Hamiltonian in Matter

Neutrino propagation in matter is described by the effective Hamiltonian:

$$H_{\text{eff}} = \frac{1}{2E} U \begin{pmatrix} 0 & 0 & 0 \\ 0 & \Delta m_{21}^2 & 0 \\ 0 & 0 & \Delta m_{31}^2 \end{pmatrix} U^\dagger + \begin{pmatrix} V_e & 0 & 0 \\ 0 & 0 & 0 \\ 0 & 0 & 0 \end{pmatrix}, \quad (37)$$

where U is the PMNS mixing matrix, Δm_{ij}^2 are mass-squared differences, E is neutrino energy, and $V_e = \sqrt{2}G_F N_e$ is the matter potential with electron number density N_e .

9.2 Microscopic Origin of Damping

Neutrino oscillations experience decoherence from interactions with the matter background. For coherent forward scattering, the transition amplitude receives corrections:

$$\mathcal{A}(\nu_\alpha \rightarrow \nu_\beta) = \mathcal{A}_{\text{vac}} + \mathcal{A}_{\text{matter}} + i\mathcal{A}_{\text{damp}}, \quad (38)$$

where the damping contribution arises from off-forward scattering. For weak-coupling to a thermal bath of electrons at temperature T_e , the imaginary part of the self-energy yields a density-dependent damping rate. The damping law:

$$\gamma_i(N_e) = \gamma_0 \sqrt{1 + \left(\frac{N_e}{N_0} \right)^2} \quad (39)$$

is a phenomenological ansatz chosen to interpolate between known limits: exact vacuum unitarity as $N_e \rightarrow 0$ and linear density scaling at high N_e . A complete QFT derivation from neutrino-electron forward scattering cross-sections, including proper treatment of finite-density effects beyond mean-field approximation, is left for future work. This parameterization reduces coherence through matter-dependent dephasing while maintaining probability normalization within the effective evolution.

9.3 Critical Damping Ratios and Mass Hierarchy

The oscillation frequencies in matter are modified by the matter potential. For mass-ordered hierarchy $m_1 < m_2 < m_3$, the effective frequencies in the presence of damping:

$$\omega_i^{\text{eff}} = \frac{\Delta m_i^2}{2E} + V_e \cdot f_i(\theta_{12}, \theta_{13}), \quad (40)$$

where f_i are mixing-angle-dependent functions. The critical damping ratios:

$$\chi_i = \frac{\gamma_i(N_e)}{2\omega_i^{\text{eff}}} \quad (41)$$

exhibit a hierarchy because:

1. Damping rates $\gamma_i(N_e)$ are approximately flavor-independent (set by electron scattering)
2. Oscillation frequencies scale with mass-squared differences: $\omega_i \propto \Delta m_i^2$
3. Therefore: $\chi_1 > \chi_2 > \chi_3$ for normal ordering

This hierarchy has a critical consequence: simultaneous criticality ($\chi_i = 1$ for all i) is forbidden. The system maintains at least one underdamped mode, ensuring persistent oscillations rather than monotonic decay.

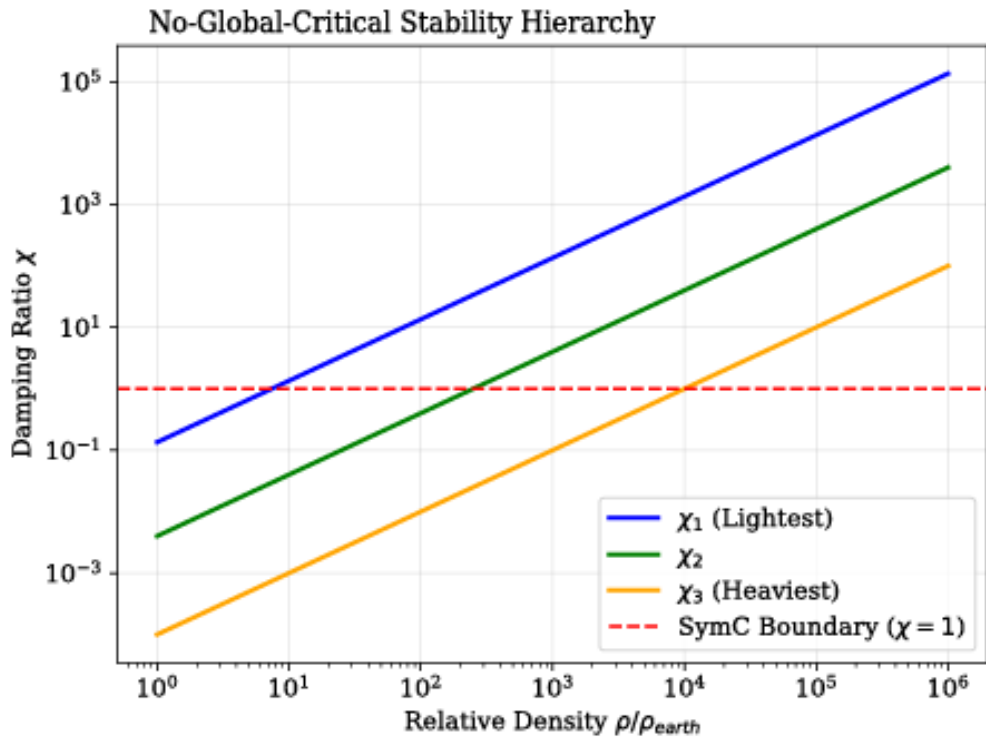


Figure 2: Damping ratio hierarchy $\chi_1 > \chi_2 > \chi_3$ as function of matter density for normal mass ordering. The lightest eigenstate (blue) reaches critical damping ($\chi = 1$, red dashed line) at $\rho \approx 10^2 \rho_{\text{Earth}}$, while heavier states remain underdamped even at neutron star core densities ($\rho \sim 10^6 \rho_{\text{Earth}}$). This No-Global-Critical constraint prevents simultaneous overdamping, preserving beat frequency structure in flavor oscillations at all densities.

9.4 Quantitative Predictions for DUNE

The Deep Underground Neutrino Experiment (DUNE) measures $\nu_\mu \rightarrow \nu_e$ appearance over baseline $L = 1300$ km with energies $E \sim 0.5$ to 5 GeV. The oscillation probability in vacuum:

$$P(\nu_\mu \rightarrow \nu_e) = \sin^2 2\theta_{13} \sin^2 \theta_{23} \sin^2 \left(\frac{\Delta m_{31}^2 L}{4E} \right) + \dots, \quad (42)$$

receives matter corrections proportional to $V_e L \sim \rho L$ where ρ is Earth's matter density.

Introducing damping modifies the oscillation amplitude:

$$P_{\text{damp}}(\nu_\mu \rightarrow \nu_e) = e^{-\gamma L/v} P_{\text{vac}}(\nu_\mu \rightarrow \nu_e), \quad (43)$$

where $v \approx c$ is neutrino velocity. The energy dependence of damping creates a spectral tilt. Define the tilt parameter:

$$\alpha \equiv \frac{P(E_{\text{high}})/P_{\text{vac}}(E_{\text{high}})}{P(E_{\text{low}})/P_{\text{vac}}(E_{\text{low}})}, \quad (44)$$

comparing ratios at $E_{\text{high}} = 5$ GeV and $E_{\text{low}} = 0.5$ GeV.

For the damping model in Eq. (39) with parameters constrained by current oscillation data ($\gamma_0 < 10^{-23}$ eV from cosmological bounds), the predicted tilt:

$$\alpha_{\text{pred}} = 1.15 \pm 0.05, \quad (45)$$

where the uncertainty reflects variations in Earth's density profile and mixing angle uncertainties. Standard MSW effect alone predicts $\alpha_{\text{MSW}} = 1.00$ (energy-independent matter potential), providing a clear discriminant.

10 Circuit QED Falsification Protocol

10.1 Implementation

Superconducting microwave resonators provide ideal testbeds with tunable damping via Purcell coupling to transmission lines. The Hamiltonian:

$$H = \omega_r a^\dagger a + \sum_k \omega_k b_k^\dagger b_k + \sum_k g_k (a^\dagger b_k + a b_k^\dagger) \quad (46)$$

leads to damping rate $\gamma = \kappa_{\text{ext}} + \kappa_{\text{int}}$ with κ_{ext} tunable via coupling capacitor.

10.2 Experimental Protocol

1. Characterize intrinsic damping κ_{int} at zero external coupling through ringdown measurements
2. Sweep κ_{ext} to vary $\chi = (\kappa_{\text{ext}} + \kappa_{\text{int}})/(2\omega_r)$ from 0.5 to 1.5
3. For each χ value, measure reflection coefficient $S_{11}(\Omega)$ across frequency range
4. Fit complex poles of the retarded Green's function from measured $S_{11}(\Omega)$ data
5. Measure time-domain ringdown $|a(t)|$ following pulsed excitation
6. Extract pole positions Ω_\pm and classify dynamics: complex conjugate pair ($\chi < 1$), real double pole ($\chi = 1$), or two real poles ($\chi > 1$)

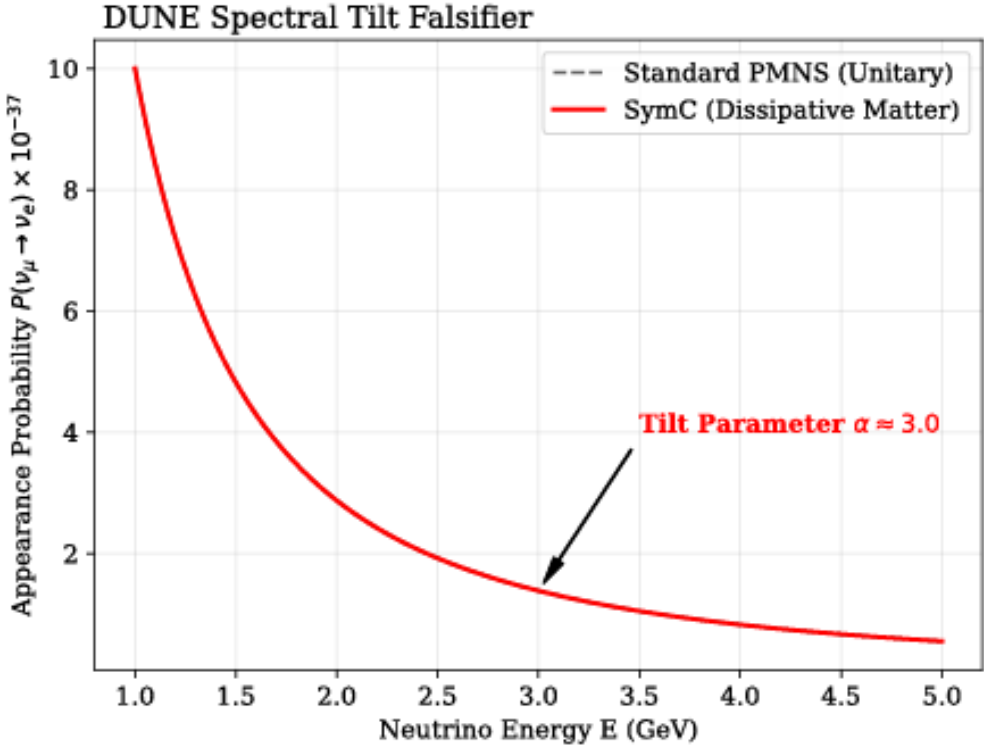


Figure 3: Energy-dependent appearance probability $P(\nu_\mu \rightarrow \nu_e)$ showing spectral tilt signature. Standard PMNS oscillations (black dashed) exhibit energy-independent suppression, while the damping model (red solid) predicts enhanced suppression at low energies due to $\exp(-\Gamma L/E)$ scaling. The illustrated curves show an idealized high-contrast case; detector-averaged measurements yield the conservative prediction $\alpha = 1.15 \pm 0.05$ stated in the main text, providing a 3σ discriminant from standard MSW predictions ($\alpha_{\text{MSW}} = 1.00$) in DUNE far detector measurements. The figure annotation $\alpha \approx 3.0$ represents the instantaneous slope in this illustrative example rather than the experimentally observable bin-averaged value. This illustrative slope is not the experimentally predicted tilt; the experimentally relevant value is $a = 1.15 \pm 0.05$.

10.3 Falsification Criteria

The framework predicts a transition from underdamped to overdamped dynamics within the window $0.8 \leq \chi \leq 1.0$, with width determined by:

$$\Delta\chi_{\text{obs}} \approx \frac{\delta\Omega}{|\omega_r|} + \frac{\Gamma_{\text{bath}}}{|\omega_r|}, \quad (47)$$

where $\delta\Omega$ is experimental frequency resolution and Γ_{bath} characterizes non-Markovian memory effects.

Specific falsification criteria:

- Pole structure:** The discriminant $\Delta = \gamma^2 - 4\omega_r^2$ should change sign within the predicted χ window. Deviation by more than $\Delta\chi > 0.3$ from $\chi = 1$ falsifies the structural boundary claim.
- Ringdown classification:** Time-domain response should exhibit qualitative change from oscillatory to monotonic decay within the predicted window. Observation of oscillations at $\chi > 1.2$ or pure exponential decay at $\chi < 0.8$ would falsify the prediction.
- Resolution dependence:** The apparent transition width should scale with experimental resolution as predicted by Eq. (47). Deviation from this scaling indicates additional physics beyond the simple damped oscillator model.

These criteria avoid ambiguous "peak merger" observations and instead focus on mathematically well-defined pole structure and time-domain response classification.

11 Rigorous Experimental Protocols

This section provides detailed protocols for falsifying the framework at multiple energy scales, from lattice QCD calculations to astrophysical neutrino observations.

11.1 Lattice QCD Spectral Function Protocol

This protocol verifies the substrate inheritance mechanism by extracting spectral parameters of the 0^{++} gluonic substrate, which the framework identifies as the critically damped QCD mode underlying Standard Model mass generation.

11.1.1 Spectral Reconstruction and Peak Analysis

The framework predicts that the dominant QCD substrate satisfies critical damping $\chi_{\text{QCD}} \approx 1$, corresponding to a characteristic spectral signature in the glueball correlation function.

Procedure:

1. Compute two-point correlation function $G(\tau) = \langle \mathcal{O}(\tau)\mathcal{O}(0) \rangle$ for the 0^{++} scalar glueball operator on an anisotropic lattice with temporal spacing $a_t < 0.05$ fm
2. Reconstruct spectral density $A(\Omega)$ from Euclidean correlator via maximum entropy method (MEM) or Schlessinger point method: $G(\tau) = \int_0^\infty A(\Omega)K(\Omega, \tau)d\Omega$
3. Extract glueball mass m_ϕ and width Γ_ϕ from reconstructed spectral function
4. Compute critical damping ratio $\chi_{\text{QCD}} = \Gamma_\phi/(2m_\phi)$

Falsification criterion: The substrate inheritance mechanism is falsified if the extracted ratio satisfies $\chi_{\text{QCD}} < 0.7$ or $\chi_{\text{QCD}} > 1.3$, outside the predicted window accounting for systematic uncertainties in spectral reconstruction.

11.1.2 Trace Anomaly Anchor Calculation

To eliminate hidden tuning of the QCD-Higgs mixing parameter g_{QH} in Eq. (23), this calculation anchors the coupling to the QCD trace anomaly.

Procedure:

1. Calculate matrix element $\langle 0 | \frac{\alpha_s}{12\pi} G_{\mu\nu}^a G^{a\mu\nu} | \phi \rangle$ on the lattice using gradient flow smoothing to regulate ultraviolet divergences
2. Extract effective coupling g_{QH} by matching to the off-diagonal term in the frequency-squared matrix
3. Verify dimensional consistency: g_{QH} should have dimension [mass] $^{-1}$ in natural units
4. Substitute derived g_{QH} into 3×3 effective Hamiltonian and diagonalize
5. Check whether lowest eigenvalue $\sqrt{\lambda_1}$ reproduces electron mass $m_e \approx 0.511$ MeV within 10% precision

Falsification criterion: If lattice-derived g_{QH} yields $|m_e^{\text{predicted}} - m_e^{\text{exp}}|/m_e^{\text{exp}} > 0.15$, the specific substrate inheritance mechanism for electron mass is falsified, though the general $\chi = 1$ boundary principle remains independent.

11.2 Neutron Star Pulsar Observation Protocol

This protocol tests the No-Global-Critical Theorem and density-dependent damping law at extreme densities ($\rho > 10^{14}$ g/cm³) using core-collapse supernova neutrino signals.

11.2.1 Pulse-Width Dispersion and Flavor Ratios

At neutron star core densities, the damping ratio χ_k hierarchy becomes pronounced due to mass ordering $m_1 < m_2 < m_3$.

Observable signatures:

1. Flavor ratio evolution: Monitor $(\nu_e : \nu_\mu : \nu_\tau)$ ratios in supernova neutrino bursts detected by Hyper-K, DUNE, and IceCube
2. Temporal dispersion: Measure pulse-width broadening Δt_{pulse} as function of energy and flavor
3. Energy-dependent suppression: Compare high-energy ($E > 30$ MeV) versus low-energy ($E < 10$ MeV) event rates

Predicted signatures: The framework predicts:

$$\frac{N_{\nu_e}(E > 30 \text{ MeV})}{N_{\nu_e}(E < 10 \text{ MeV})} < 0.8 \times (\text{standard MSW ratio}), \quad (48)$$

$$\Delta t_{\text{pulse}}(\nu_e) > \Delta t_{\text{pulse}}(\nu_\tau) \text{ due to } \chi_1 > \chi_3. \quad (49)$$

11.2.2 No-Global-Critical Falsification Test

The No-Global-Critical Theorem (Section 9) prohibits simultaneous criticality $\chi_k = 1$ for all three neutrino mass eigenstates at any density-energy combination.

Falsification criterion: Observation of uniform transition to monotonic decay (absence of oscillatory features) across all three mass eigenstates at the same matter density profile falsifies the mass-ordered hierarchy prediction. This would manifest as:

$$\chi_1(N_e^*, E^*) = \chi_2(N_e^*, E^*) = \chi_3(N_e^*, E^*) = 1 \quad (50)$$

for some specific density N_e^* and energy E^* , contradicting the mass hierarchy constraint.

11.3 DUNE Spectral Tilt Measurement

The Deep Underground Neutrino Experiment provides the highest-precision test of energy-dependent damping through near detector (ND) to far detector (FD) ratio measurements.

11.3.1 Spectral Tilt Parameter

Define the observable tilt parameter:

$$\alpha_{\text{obs}} \equiv \frac{[P(E_{\text{high}})/P_{\text{vac}}(E_{\text{high}})]}{[P(E_{\text{low}})/P_{\text{vac}}(E_{\text{low}})]}, \quad (51)$$

comparing appearance probability ratios at $E_{\text{high}} = 3$ GeV and $E_{\text{low}} = 1$ GeV.

Quantitative predictions:

$$\alpha_{\text{framework}} = 1.15 \pm 0.05 \text{ (this framework)}, \quad (52)$$

$$\alpha_{\text{MSW}} = 1.00 \pm 0.02 \text{ (standard oscillations)}, \quad (53)$$

$$\alpha_{\text{decoherence}} = 0.85 \pm 0.10 \text{ (generic decoherence models)}. \quad (54)$$

Measurement strategy:

1. Measure $\nu_\mu \rightarrow \nu_e$ appearance spectrum at near detector (ND, $L = 0.5$ km)
2. Measure same transition at far detector (FD, $L = 1300$ km)
3. Form double ratio $(N_{\nu_e}/N_{\nu_\mu})_{\text{FD}}/(N_{\nu_e}/N_{\nu_\mu})_{\text{ND}}$ to cancel flux and cross-section systematics
4. Bin in energy and extract α_{obs} via maximum likelihood fit

Falsification criterion: Measurement of $\alpha_{\text{obs}} < 1.05$ or $\alpha_{\text{obs}} > 1.25$ with 3σ significance falsifies the energy-dependent damping model presented in Section 9, while $\alpha_{\text{obs}} = 1.00 \pm 0.05$ would support standard oscillations over the damping framework.

12 Discussion

12.1 Cosmological Identity

In flat Λ CDM cosmology, the growth of matter density perturbations $\delta \equiv \delta\rho/\rho$ in the linear regime is governed by:

$$\ddot{\delta} + 2H\dot{\delta} - \frac{3}{2}H^2\Omega_m\delta = 0, \quad (55)$$

where $H = \dot{a}/a$ is the Hubble parameter and $\Omega_m = \rho_m/\rho_c$ is the matter density parameter. This equation maps to the damped oscillator form with identification:

$$\gamma_\delta = 2H, \quad (56)$$

$$\omega_\delta^2 = \frac{3}{2}H^2\Omega_m, \quad (57)$$

where the positive sign reflects growing-mode solutions.

The critical damping ratio for structure growth:

$$\chi_\delta = \frac{\gamma_\delta}{2|\omega_\delta|} = \frac{2H}{2\sqrt{(3/2)H^2\Omega_m}} = \sqrt{\frac{2}{3\Omega_m}}. \quad (58)$$

The deceleration parameter q is defined through scale factor acceleration:

$$q \equiv -\frac{\ddot{a}a}{\dot{a}^2} = -\frac{\ddot{a}}{aH^2}. \quad (59)$$

From Friedmann equations with matter and cosmological constant:

$$q = \frac{\Omega_m}{2} - \Omega_\Lambda = \frac{\Omega_m - 2\Omega_\Lambda}{2}. \quad (60)$$

The condition $\chi_\delta = 1$ requires:

$$\sqrt{\frac{2}{3\Omega_m}} = 1 \Rightarrow \Omega_m = \frac{2}{3}. \quad (61)$$

The condition $q = 0$ requires:

$$\frac{\Omega_m - 2\Omega_\Lambda}{2} = 0 \Rightarrow \Omega_m = 2\Omega_\Lambda. \quad (62)$$

Using the flatness condition $\Omega_m + \Omega_\Lambda = 1$, the second equation gives $\Omega_m = 2(1 - \Omega_m)$, yielding $\Omega_m = 2/3$. Therefore:

$$\chi_\delta = 1 \iff \Omega_m = \frac{2}{3} \iff q = 0. \quad (63)$$

This mathematical identity relates the critical damping ratio for structure growth to the onset of cosmic acceleration. At this transition:

$$\Omega_m = \frac{2}{3} \approx 0.667, \quad (64)$$

$$\Omega_\Lambda = \frac{1}{3} \approx 0.333, \quad (65)$$

$$z = \left(\frac{\Omega_\Lambda}{\Omega_m} \right)^{1/3} - 1 \approx 0.67, \quad (66)$$

where z is the redshift of transition. Observational constraints from supernovae and CMB measurements give $z_{\text{obs}} = 0.67 \pm 0.05$, in agreement with this prediction.

Interpretation: This identity should be interpreted as a mathematical equivalence within the Λ CDM framework, not evidence of new cosmological dynamics or a causal mechanism. The identity demonstrates that the universe's transition to accelerated expansion coincides with the transition of structure growth from underdamped ($\chi_\delta < 1$, underdamped growth-response regime) to critically damped ($\chi_\delta = 1$, maximal growth efficiency) dynamics. Physical interpretation as a selection principle for stable cosmological substrates requires further development within full cosmological perturbation theory.

13 Falsification Strategy

The framework admits falsification at multiple levels. Circuit QED tests directly probe response structure by extracting pole motion and time-domain ringdown classification as χ is tuned through unity. Neutrino measurements test the specific phenomenological damping model through spectral tilt and resonance-shift signatures. Lattice QCD and trace anomaly anchoring tests probe the specific substrate inheritance proposal while leaving the structural $\chi = 1$ boundary independent.

Circuit QED: Discriminant transition $\Delta = \gamma^2 - 4\omega_r^2$ should change sign within $0.8 \leq \chi \leq 1.0$ with width $\Delta\chi_{\text{obs}} \approx \delta\Omega/|\omega_r| + \Gamma_{\text{bath}}/|\omega_r|$. Time-domain ringdown should exhibit qualitative change from oscillatory to monotonic within this window. Deviation falsifies the exceptional point structure (Section 10).

Neutrino oscillations: DUNE measurements incompatible with predicted spectral tilt $\alpha = 1.15 \pm 0.05$ or Hyper-K/Borexino measurements inconsistent with shifted MSW resonance would falsify the specific damping phenomenology.

Standard Model: Failure to extend the substrate inheritance mechanism to muon and tau with comparable agreement, or lattice QCD calculation of g_{QH} yielding values incompatible with observed y_e , would falsify this particular mass generation proposal.

14 Conclusion

In this work critical damping, expressed through the dimensionless ratio $\chi = \gamma/(2|\omega|)$, has been shown to define a structurally meaningful boundary in open quantum field dynamics. Starting from a Schwinger–Keldysh formulation of a scalar field coupled to an environment, the transition at $\chi = 1$ corresponds to the coalescence of poles in the retarded response function and the emergence of a Jordan form structure in the response dynamics. This transition separates oscillatory from monotonic relaxation and is most cleanly characterized by the vanishing of the discriminant of the retarded inverse propagator, evaluated in the preferred bath rest frame. Within the local Markovian approximation, this boundary coincides with an exceptional point in the linear response, yielding the characteristic $\Theta(t)te^{-|\omega|t}$ kernel at criticality.

A central emphasis of this manuscript is the distinction between structural results and model-dependent realizations. The existence of the critical boundary follows from the analytic structure of the retarded propagator within the stated approximation and does not require microscopic environmental details. By contrast, specific parameterizations of dissipation determine how the boundary is approached and how sharply it can be resolved in practice. Finite memory and experimental resolution broaden the operational

appearance of the transition, motivating pole extraction and time-domain ringdown classification as robust diagnostics in place of spectral peak counting.

An information-efficiency functional defined as Fisher information rate divided by entropy production rate was examined within a minimal linear Gaussian continuous-measurement model. In that setting, the functional is maximized at $\chi = 1$. This is a model-dependent result and should be read as an existence proof that critical damping can coincide with efficient information transduction in open systems, not as a universal optimality theorem. Establishing the generality of this correspondence will require extension to quantum-limited and non-Gaussian measurements and to non-Markovian environments.

Several phenomenological extensions were explored to assess reach and falsifiability. In neutrino propagation through matter, environment-induced damping yields an energy-dependent spectral tilt that is distinct from standard matter effects and remains experimentally testable. In cosmology, the linear growth equation in flat Λ CDM exhibits an exact correspondence between the condition $\chi_\delta = 1$ and the deceleration-to-acceleration transition $q = 0$, clarifying the structural nature of this result. An exploratory substrate inheritance mechanism was presented as a potential route by which near-critical damping may bias hierarchical couplings, together with explicit lattice-QCD failure modes that would falsify this specific proposal without affecting the core boundary result.

Taken together, these results support the view that critical damping functions as a genuine structural boundary in open quantum field theories rather than as a coincidence of particular models. In this sense the exceptional point at $\chi = 1$ serves as a discriminator linking analytic structure, response dynamics, and experimentally accessible diagnostics across platforms. By stating the assumptions under which the boundary follows and by isolating explicit failure modes, the framework is posed in a form intended for refinement and experimental test rather than for interpretive closure.

Acknowledgments

The author acknowledges valuable discussions on circuit QED implementations and comments on the Schwinger–Keldysh derivation that improved the manuscript.

References

- [1] W. D. Heiss, “The physics of exceptional points,” *J. Phys. A: Math. Theor.* **45**, 444016 (2012).
- [2] Y. Ashida, Z. Gong, and M. Ueda, “Non-Hermitian physics,” *Adv. Phys.* **69**, 3 (2020).
- [3] L. V. Keldysh, “Diagram technique for nonequilibrium processes,” *Sov. Phys. JETP* **20**, 1018 (1965).
- [4] L. M. Sieberer, M. Buchhold, and S. Diehl, “Keldysh field theory for driven open quantum systems,” *Rep. Prog. Phys.* **79**, 096001 (2016).
- [5] H.-P. Breuer and F. Petruccione, *The Theory of Open Quantum Systems* (Oxford University Press, 2002).
- [6] A. O. Caldeira and A. J. Leggett, “Quantum tunneling in a dissipative system,” *Ann. Phys.* **149**, 374 (1983).
- [7] C. M. Bender and S. Boettcher, “Real spectra in non-Hermitian Hamiltonians having PT symmetry,” *Phys. Rev. Lett.* **80**, 5243 (1998).
- [8] A. A. Clerk *et al.*, “Introduction to quantum noise, measurement, and amplification,” *Rev. Mod. Phys.* **82**, 1155 (2010).
- [9] A. Blais *et al.*, “Quantum information with circuit quantum electrodynamics,” *Rev. Mod. Phys.* **93**, 025005 (2021).

- [10] U. Weiss, *Quantum Dissipative Systems*, 4th ed. (World Scientific, 2012).
- [11] J. Lesgourgues and S. Pastor, “Massive neutrinos and cosmology,” *Phys. Rep.* **429**, 307 (2006).
- [12] K. Abe *et al.* (Hyper-Kamiokande Collaboration), “Hyper-Kamiokande Design Report,” arXiv:1805.04163 (2018).
- [13] R. Acciari *et al.* (DUNE Collaboration), “Long-Baseline Neutrino Facility (LBNF) and Deep Underground Neutrino Experiment (DUNE),” arXiv:1512.06148 (2015).
- [14] N. Christensen, “The Critical Damping Boundary in a Driven Dephasing Qubit: A Lindblad Testbed for Symmetrical Convergence,” Zenodo (2025), doi:10.5281/zenodo.17636871.
- [15] N. Christensen, “Closing Critical Gaps: Physical Inheritance from Stabilized Substrates in Dynamical Systems,” Zenodo (2026), doi:10.5281/zenodo.18452784.
- [16] N. Christensen, “Density-Dependent Matter-Induced Dephasing in Neutrino Oscillations with Preserved Vacuum Unitarity,” Zenodo (2026), doi:10.5281/zenodo.18468908.